Supporting Information

Synthesis and Application of CeO_2/SnS_2 Heterostructures as Highly-Efficient Coreaction Accelerator in Luminol-Dissolved O_2 System for Ultrasensitive Biomarkers Immunoassay

Lei Yang,† Yue Jia,† Dan Wu,† Yong Zhang,† Huangxian Ju,†,‡ Yu Du,†,* Hongmin Ma,†,* Qin Wei†

† Key Laboratory of Interfacial Reaction & Sensing Analysis in Universities of Shandong, School of Chemistry and Chemical Engineering, University of Jinan, Jinan 250022, China

‡ State Key Laboratory of Analytical Chemistry for Life Science, School of Chemistry and Chemical Engineering, Nanjing University, Nanjing 210023, China.

* Corresponding author

Tel.: +86 531 82765730;

Fax: +86 531 82765969;

E-mail: sdjndxdy@163.com; mahongmin2002@126.com

Contents:

S1. Materials and regents

S2. Apparatus

S3. Molar structure of HWR

S4. SEM images of pure SnS_2 NSs and CeO_2 NPs

S5. XPS spectra analysis of CeO_2/SnS_2

S6. FT-IR spectra analysis of CeO_2/SnS_2 and amine-functionalized CeO_2/SnS_2

S7. Electrochemical characterization of the biosensor

S8. Evidence of $O_2^{\bullet-}$ existence by Tiron test

S9. Optimization of experimental conditions

S10. Comparison of proposed method with other reported methods for NT-proBNP detection

S1. Materials and reagents.

Luminol, horse spleen ferritin (100 mg/mL) and bovine serum albumin (BSA) (96–99%) were purchased from Sigma-Aldrich Co. (St. Louis, MO, USA). $SnCl_4 \cdot 5H_2O$, $Ce(NO_3)_3 \cdot 6H_2O$, thioacetamide (CH_3CSNH_2), cetyltrimethyl ammonium bromide (CTAB), 3-aminopropyltriethoxysilane (APTES), Tiron (1,2-dihydroxy-3,5-benzenedisulfonic acid disodium salt) were obtained from Shanghai Reagent Company (Shanghai, China). The NT-proBNP, capture-antibody (Ab_1), detection antibody (Ab_2), PCT, CEA, insulin and PSA antigen were all purchased from GenScript Biotech Corporation. (Nanjing, China). HWRGWVC heptapeptide (HWR) was ordered from GL Biochem. Ltd. (Shanghai, China). All of the other chemicals were of analytical reagent grade and were used without further purification. Phosphate buffered saline (PBS) was prepared by using 0.1 M Na_2HPO_4 and 0.1 M KH_2PO_4 solution. 2.5 mM $K_3Fe(CN)_6/K_4Fe(CN)_6$ and 0.1 M KNO_3 solution were used as electrolyte for electrochemical impedance spectroscopy (EIS). Deionized water (18.25 MΩ/cm, 24 °C) was used for all of the experiments.

S2. Apparatus. Scanning electron microscope (SEM) images was obtained by a field emission SEM (Zeiss, Germany). High resolution transmission electron microscope (HRTEM) and TEM images were obtained by JEOL JEM-2100F (Japan). The Lambda 35 UV-vis Spectrometer (Perkin-Elmer, United States) was used to complete the UV-vis absorption spectrum. The D8 focus diffractometer (Bruker AXS, Germany) was used to complete the X-ray diffraction (XRD) patterns. The ECL measurements were performed with a MPI-F flow-injection ECL detector (Xi'an remax Electronic Science Tech. Co. Ltd., China) and electrochemical measurements were carried out on electrochemical workstation (Zahner Zennium PP211, Germany) using a three-electrode system which is made up of a platinum wire as an auxiliary electrode, an Ag/AgCl electrode as reference electrode, and GCE (4 mm in diameter) as working electrode.

High performance liquid chromatography (HPLC) was performed with an Agilent 1260 HPLC system consisting of an UV detector and a Zorbax C18 column (4.6 × 250 mm, 5 μm). Samples were eluted by the use of a mobile phase of acetonitrile/water (30:70, v/v). For the mobile phase, the injection volume was 10 uL with a flow rate of 0.5 mL/min, and the wavelength was set to 220 nm.

Circular dichroism (CD) spectrum was obtained by Applied Photophysics. Ltd (Britain). All the CD spectra were obtained by scanning from 190 to 260 nm utilizing a MOS-450 spectrometer consisting of a quartz cuvettes of 1 mm optical path length at 25 ^{o}C. All the data were expressed in terms of mean residual ellipticity (h) in deg cm^{2} dmol^{-1}.

S3. Molar structure of HWR.

By modifying with a cysteine to the C-terminus of HWRGWV hexapeptide, HWRGWVC heptapeptide (HWR) was obtained whose structure was illustrated as follows:[1]

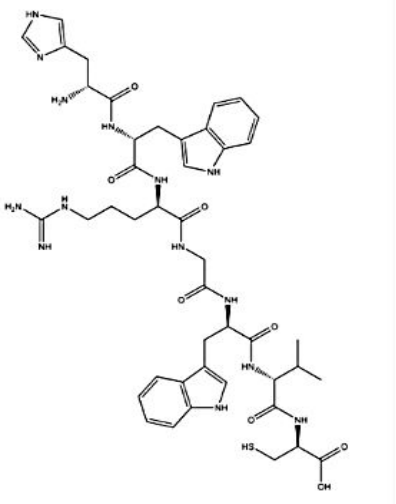

S.4 SEM images of pure SnS_2 NSs and CeO_2 NPs.

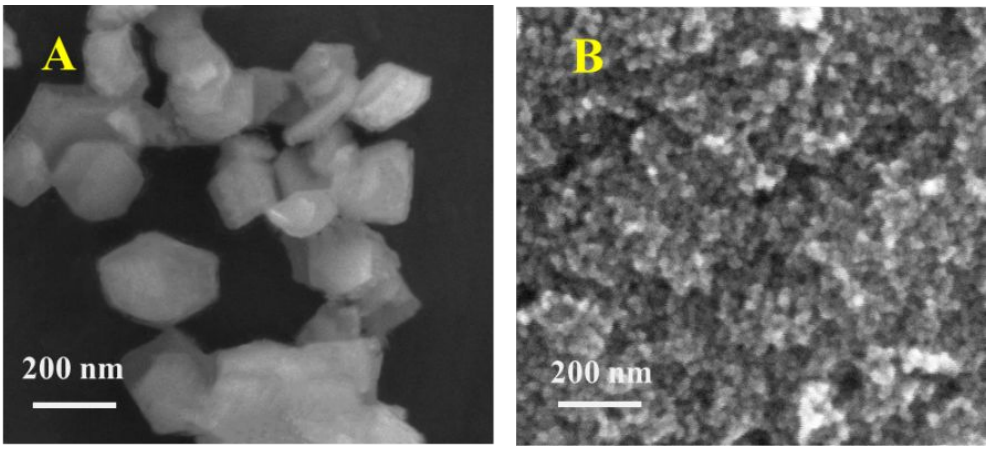

Figure S1. SEM images of pure SnS_2 NSs (A) and CeO_2 NPs (B)

S.5 XPS spectra analysis of CeO_2/SnS_2. To further investigate the surface structure and the binding nature of the elements of composites, the XPS spectra of CeO_2/SnS_2 have been provided in Figure S2. The Sn 3d spectrum in Figure S2A shows two peaks from 484 to 498 eV, which corresponds to Sn $3d_{5/2}$ region and Sn $3d_{3/2}$ region. Thus, the chemical state of Sn in the composite is Sn^{4+}. In addition, as shown in Figure S2B, the binding energies of S $2p_{3/2}$ and S $2p_{1/2}$ can be observed at about 162.38 and 163.48 eV, which are consistent with the reference values for SnS_2 crystal. For the Ce $3d_{5/2}$ and Ce $3d_{3/2}$ (Figure S2C), the peak at the binding energy side (886.38 eV and 905.4 eV) are the signs of the Ce^{3+} while the peak at the 898.7 eV is the sign of Ce^{4+}.[2] The O 1s region was provided in Figure S2D, which was attributed to the metal-oxygen bond were obtained.

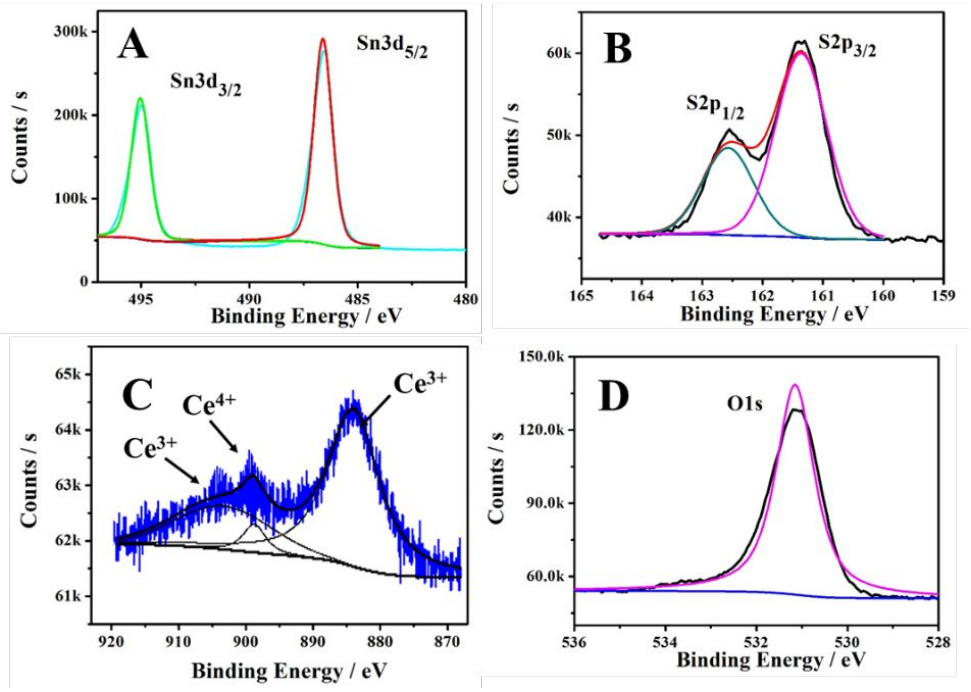

Figure S2. XPS spectra of Sn 3d region (A), S 2p region (B), Ce 3d region (C) and O 1s region (D).

S6. FT-IR spectra analysis of CeO_2/SnS_2 and amine-functionalized CeO_2/SnS_2. To prove the successful amine-functionalization of APTES on CeO_2/SnS_2 surface, FT-IR spectra of CeO_2/SnS_2 and amine-functionalized CeO_2/SnS_2 were displayed in Figure S3. Compared to pure CeO_2/SnS_2, characteristic aliphatic C-H absorbance at 2935 cm^{-1} and 2865 cm^{-1} were observed in amine-functionalized CeO_2/SnS_2, which indicated the functional organosilane were modified onto CeO_2/SnS_2 surface.[3] Combining with the N-H stretching vibration absorbance at 3435 cm^{-1}, it can be conclude that CeO_2/SnS_2 has been successfully functionalized by APTES with amino groups.

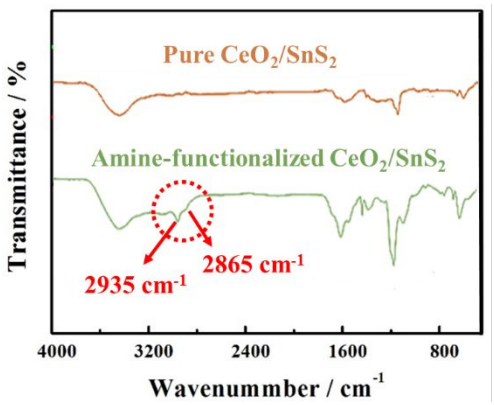

Figure S3. FT-IR spectra of CeO_2/SnS_2 and amine-functionalized CeO_2/SnS_2.

S7. Electrochemical characterization of the biosensor. Stepwise characterization of the proposed biosensor was confirmed with EIS and CV profiles conducted in $[Fe(CN)_6]^{4-/3-}$ (5 mmol/L) solution containing KCl (0.1 mol/L). Impedance spectra of GCE at different modified steps was shown in Figure S4A. GCE/CeO_2/SnS_2-HWR (curve a) showed a slightly increased semicircle compared with bare GCE (curve b), proving the excellent electrical conductivity of CeO_2/SnS_2. After the continuous modifications of nonconductive Ab_1, BSA, Ag and Lum@Ft-Ab_2 on the GCE surface, resistance (curve c, d, e and f) increased sequentially due to their poor conductivity of proteins. All the results above were consistent with the CV profiles in Figure S4B, indicating the superficial construction of the proposed ECL biosensor was successful.

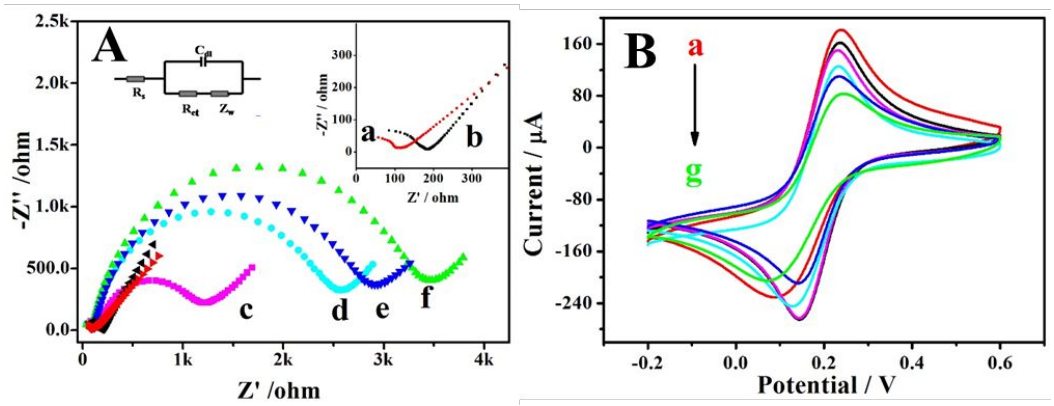

Figure S4. EIS (A) and corresponding CV curves of the stepwise characterization of the proposed biosensor.

S8. Evidence of $O_2^{\bullet-}$ existence by Tiron test.

As a specific $O_2^{\bullet-}$ scavenger, Tiron (1,2-dihydroxy-3,5-benzenedisulfonic acid disodium salt) was used to eliminate the $O_2^{\bullet-}$ that produced from the reaction, which could hinder the ECL emission of luminol. As displayed in Figure S5A, when adding 1 mmol/L of Tiron solution into the PBS electrolyte (pH 8.0), the ECL intensity decreased from 15530 a.u. to 4180 a.u. while there's no apparent decease of the corresponding current (Figure S5B). It indicated that it was the $O_2^{\bullet-}$ elimination by Tiron induced the ECL signal decrease instead of the blocking of electron transport, revealing the existence and necessity of $O_2^{\bullet-}$ during the ECL emission of luminol.

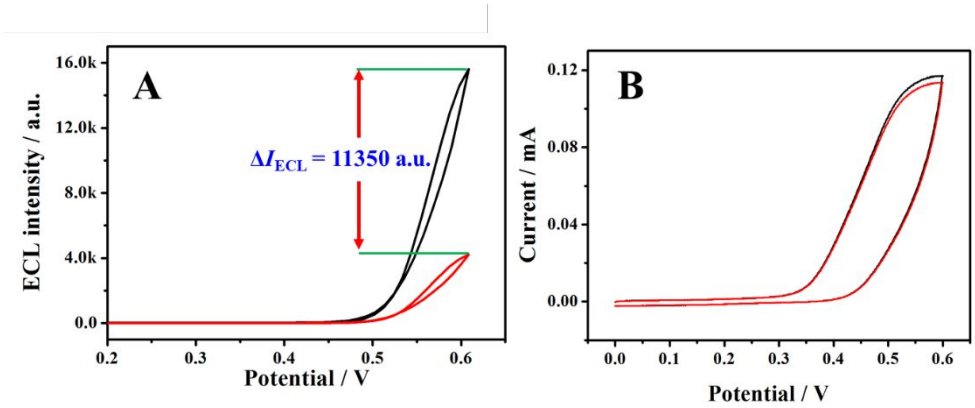

Figure S5. (A) ECL-potential curve of biosensors detected in electrolyte with (red curve) and without 20 mmol/L Tiron (black curve) solution, (B) corresponding CV curves of (A).

S9. Optimization of experimental conditions.

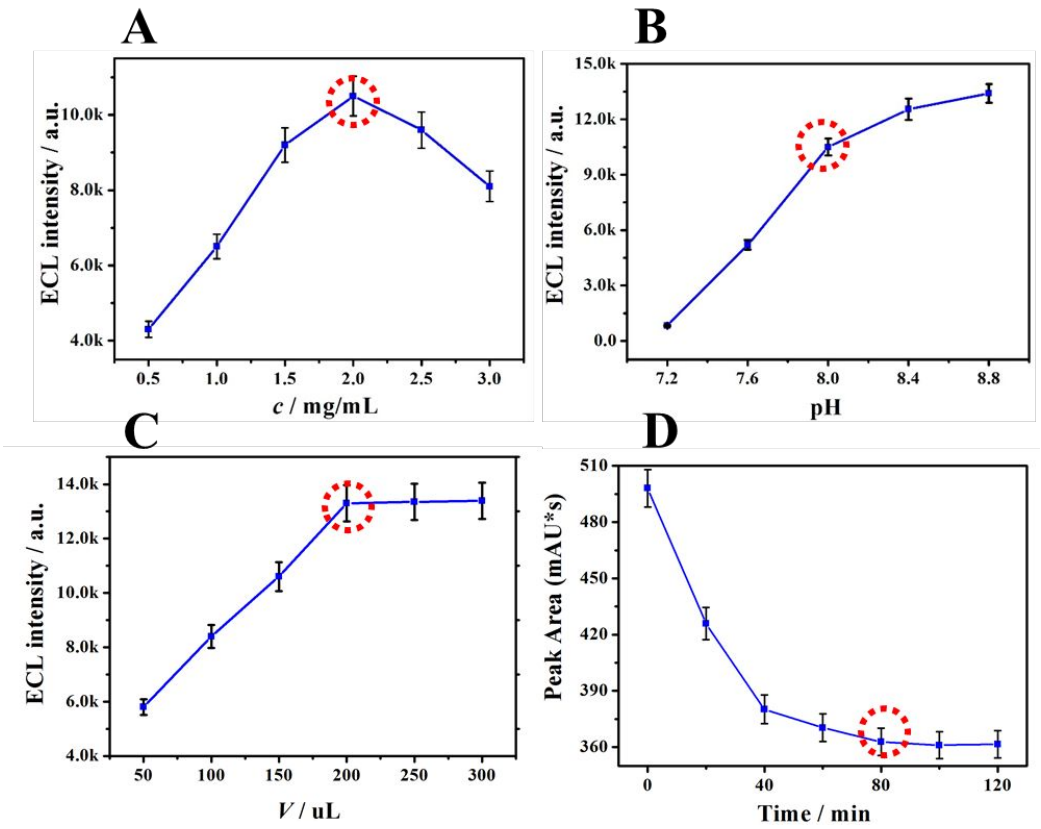

Figure S6. Optimizations of the (A) CeO_2/SnS_2 concentration, (B) pH values of PBS solution, (C) volume of added luminol solution (10 mmol/L), (D) incubation time of HWR.

Optimized experiment conditions play a crucial role in the ECL detection which contributes to obtain satisfying ECL responses.[4] Concentration of CeO_2/SnS_2, pH value of the PBS solution, the added volume of luminol (10 mmol/L), the HWR incubation time were discussed sequentially to obtain the optimal conditions. Firstly, the concentration of CeO_2/SnS_2 was optimized to be 2 mg/mL according to the maximum ECL intensity in Figure S6A. Then, 0.1 mol/L PBS with different pH values (from 7.2

to 8.8) were investigated. As shown in Figure S6B, pH value of PBS was optimized to 8.0 considering the negative effects of basic environment to the biological activity of biomolecules, and the ECL intensity in pH 8.0 PBS totally met the detection requirements as well. Then, the volume of added luminol was optimized. As shown in Figure S6C, the ECL intensity levelled off when the luminol volume was 200 μL, thus the optimized luminol volume was 200 μL for Lum@Ft fabrication. HPLC was used to prove the efficient combination of HWR with CeO_2/SnS_2 via amide bond. First of all, 1 mL of CeO_2/SnS_2 solution (2 mg/mL) were mixed with 1 mL of HWR solution (50 ng/mL) and coupled for different time at 4 °C. After centrifugation, the supernatants were collected for HLPC test and corresponding peak areas of HWR were recorded. As shown in Figure S6D, the curves levelled off at 80 min and kept constant, and thus the HWR incubation time was optimized to be 80 min.

S10. Table S1. Comparison of proposed method with other reported methods for NT-proBNP detection.[5-8]

Methods	Linear range (ng/mL)	Detection limit (pg/mL)	Ref
microfluidic immunoassay	0.005 — 4	3.0	5
electrochemical assay	0.02 — 100	6.0	6
ECL assay	0.0005—100	0.28	7
ECL assay	0.1 —25	0.05	8
ECL assay	0.0001 — 50	0.036	this work

Reference

(1) Yang, L.; Fan, D.; Zhang, Y.; Ding, C.; Wu, D.; Wei, Q.; Ju, H., Ferritin-Based Electrochemiluminescence Nanosurface Energy Transfer System for Procalcitonin Detection Using HWRGWVC Heptapeptide for Site-Oriented Antibody Immobilization. *Anal Chem.* **2019**, *91*, 7145-7152.

(2) Kwon, H. J.; Kim, D.; Seo, K.; Kim, Y. G.; Han, S. I.; Kang, T.; Min, S.; Hyeon, T., Ceria Nanoparticle Systems for Selective Scavenging of Mitochondrial, Intracellular, and Extracellular Reactive Oxygen Species in Parkinson's Disease. *Angew. Chem. Int. Ed.*, **2018**, *57*, 9408-9412.

(3) Wang, X.; Wang, T.; Liu, D.; Guo, J.; Liu, P., Synthesis and Electrochemical Performance of CeO_2/PPy Nanocomposites: Interfacial Effect. *Ind. Eng. Chem. Res.* **2016,** *55* (4), 866-874.

(4) Wang, J. X.; Zhuo, Y.; Zhou, Y.; Wang, H. J.; Yuan, R.; Chai, Y. Q., Ceria Doped Zinc Oxide Nanoflowers Enhanced Luminol-Based Electrochemiluminescence Immunosensor for Amyloid-beta Detection. *ACS Appl. Mater. Interfaces.* **2016,** *8* (20), 12968-12975.

(5) Liang, W.; Li, Y.; Zhang, B.; Zhang, Z.; Chen, A.; Qi, D.; Yi, W.; Hu, C., A Novel Microfluidic Immunoassay System based on Electrochemical Immunosensors: an Application for the Detection of NT-proBNP in Whole Blood. *Biosens. Bioelectron*. **2012,** *31* (1), 480-485.

(6) Zhuo, Y.; Yi, W. J.; Lian, W. B.; Yuan, R.; Chai, Y. Q.; Chen, A.; Hu, C., Ultrasensitive Electrochemical Strategy for NT-proBNP Detection with Gold Nanochains and Horseradish Peroxidase Complex Amplification. *Biosens. Bioelectron*. **2011,** *26* (5), 2188-2193.

(7) Shi, L.; Li, X.; Zhu, W.; Wang, Y.; Du, B.; Cao, W.; Wei, Q.; Pang, X., Sandwich-Type Electrochemiluminescence Sensor for Detection of NT-proBNP by Using High Efficiency Quench Strategy of Fe_3O_4@PDA toward $Ru(bpy)_3^{2+}$ Coordinated with Silver Oxalate. *ACS Sens.* **2017,** *2* (12), 1774-1778.

(8) Liu, Y.; Wang, H.; Xiong, C.; Chai, Y.; Yuan, R. An Ultrasensitive Electrochemiluminescence Immunosensor for NT-proBNP based on Self-Catalyzed Luminescence Emitter Coupled with PdCu@Carbon Nanohorn Hybrid. *Biosens. Bioelectron*. **2017,** *87*, 779-785